ADVANCED MATERIALS

Supporting Information

for *Adv. Mater.*, DOI: 10.1002/adma.201705651

Extrusion-Based 3D Printing of Hierarchically Porous Advanced Battery Electrodes

Steven D. Lacey, Dylan J. Kirsch, Yiju Li, Joseph T. Morgenstern, Brady C. Zarket, Yonggang Yao, Jiaqi Dai, Laurence Q. Garcia, Boyang Liu, Tingting Gao, Shaomao Xu, Srinivasa R. Raghavan, John W. Connell, Yi Lin, and Liangbing Hu**

Supporting Information

Extrusion-based 3D Printing of Hierarchically Porous Advanced Battery Electrodes

Steven D. Lacey[a], Dylan J. Kirsch[a], Yiju Li[a], Joseph T. Morgenstern[a], Brady C. Zarket[b], Yonggang Yao[a], Jiaqi Dai[a], Laurence Q. Garcia[c], Boyang Liu[a], Tingting Gao[a], Shaomao Xu[a], Srinivasa R. Raghavan[b], John W. Connell[c], Yi Lin[d,*], Liangbing Hu[a,*]

[a]Department of Materials Science and Engineering, University of Maryland, College Park, MD 20742-4111, USA
[b]Department of Chemical and Biomolecular Engineering, University of Maryland, College Park, MD, 20742-4111, USA
[c]Advanced Materials and Processing Branch, NASA Langley Research Center, Mail Stop 226, Hampton, VA 23681-2199, USA
[d]National Institute of Aerospace, 100 Exploration Way, Hampton, VA 23666-6147, USA

*Correspondence to Yi Lin and Liangbing Hu: yi.lin-1@nasa.gov; binghu@umd.edu

Materials & Methods

Synthesis of holey graphene (hG): The hG starting material was prepared by a facile one-step oxidation procedure developed in our laboratories. Approximately 1.5 g of commercial graphene powder (Vor-X, Vorbeck Materials; grade, reduced 070; lot, BK-77x) was placed in an alumina boat and heated to 430°C at 10°C min^{-1} in an open-ended tube furnace (OTF-1200X, MTI Corporation). After a 10h hold at 430°C, the as-prepared hG (bulk density of ~6 mg cm^{-3}) was obtained and used directly to synthesize hGO via liquid-phase oxidation.

Synthesis of holey graphene oxide (hGO) & non-nanoporous GO-based materials: The highly nanoporous hGO (bulk density of 130 mg cm^{-3}) was synthesized using an abbreviated version of the modified Hummer's method. This specific liquid-phase oxidation procedure, referred to as the simplified Hummer's method, is described in this work for the first time. First, the as-prepared hG (400 mg), sodium nitrate (200 mg; >99.0% $NaNO_3$, Sigma Aldrich) and sulfuric acid (60 mL) were added to a 100 mL flask inside a cold water bath and magnetically stirred for 15 mins. ~600

mg of potassium permanganate (2.4 g in total; $KMnO_4$, low in mercury, ACS, 99.0% min Alfa Aesar) was added to the solution every 5 mins before transferring the flask to a ~38°C bath. After a 5 h reaction, the flask was left to cool in a cold water bath for 15 mins. Hydrogen peroxide (30%) was then added to the solution in 0.2 mL increments until the residual KMnO4 was neutralized. The dark brown solution was centrifuged (3000rpm for 15 mins) a couple times with deionized (DI) water as well as a mixture of hydrochloric acid and DI water. Additional DI centrifuging steps were performed until all the acid was removed from the final hGO product. The hGO material was then freeze-dried (Labconco FreeZone 2.5 Benchtop Freeze Dry System) overnight and directly used to prepare additive-free and aqueous 3D printable inks. Note that the aforementioned simplified Hummer's method can create scalable quantities of hGO (>1 g) by increasing the batch size and subsequent chemical quantities. Additionally, the GO from Vor-X graphene material was synthesized using the simple Hummer's method described in this work; however, the GO from natural graphite was prepared using the conventional modified Hummer's method, which includes mechanical exfoliation of the starting material, graphite, followed by liquid-phase oxidation.

Ink Preparation & 3D Printing Procedure: An additive-free and highly concentrated hGO ink (~100 mg mL^{-1}) was prepared by adding DI water to the freeze-dried hGO material. The hGO slurry was mixed thoroughly with a mortar and pestle before placing the ink into a syringe tube with a 203.2 μm tip diameter for the printing process. The ink flow was controlled by an air-powered fluid dispenser (DSP501N, Fisnar) and used to print trilayer hGO mesh structures on glass slides with a line spacing of 0.8 mm. Note that the nozzle pressure and move speed were altered to achieve optimal printing of the hGO mesh structures with our lab's benchtop 3D printer. After 3D printing, the electrodes were freeze-dried in a Labconco FreeZone 2.5 Benchtop Freeze Dry System to remove the aqueous solvent and retain the printed structure. In terms of scalability

and manufacturing, the relatively slow 3D printing speed (typical speed of 1 mm s^{-1} with our benchtop 3D printer) is the limiting factor. However, for industrial purposes, the rheological properties of the reported GO-based inks would likely be tuned to meet the standards of high-throughput manufacturing (i.e. increased printing speed, etc.) and produce the desired complex 3D architectures. Note that freeze drying is widely used industrially (e.g. pharmaceuticals and food) for the scalable production of products and thus, would not be a major challenge from a manufacturing point of view.

Material Characterization: Transmission electron microscopy (TEM) and HRTEM images were acquired using a JEM 2100 LaB_6 and a JEM 2100 field emission TEM/STEM microscope, respectively. Scanning electron microscopy (SEM) was conducted on both a Hitachi SU-70 field emission microscope equipped with an energy dispersive spectrometer (EDS) and a TESCAN XEIA3 field emission microscope. A Horiba Jobin Yvon LabRam ARAMIS Raman spectrometer with a 532 nm excitation source was used to obtain the spectra for hG, all GO-based powders and discharged/charged r-hGO meshes. Fourier transform infrared spectroscopy (FTIR) measurements were conducted on a Thermo Nicolet 6700 spectrometer with a DTGS/KBr detector and diamond ATR. Rheological characterization was performed on a TA Instruments AR 2000 stress-controlled rheometer. All steady-shear and dynamic rheological tests were performed utilizing a 20 mm stainless steel parallel plate fixture at 25°C. Dynamic stress sweeps were performed at a constant angular frequency of 6.283 rad s^{-1}. Dynamic frequency sweeps were done at a constant strain amplitude within the linear viscoelastic regime of each sample. X-ray photoelectron spectroscopy (XPS) was conducted using a PHI 5000 Versaprobe III scanning XPS microprobe (ULVAC-PHI, Inc.).

Fabrication of Vacuum Filtrated and Mesh Electrodes: Vacuum filtrated (VF) hGO films were created by bath sonicating (2.5 h) and ultrasonicating (5 min at 35% amplitude) an hGO solution before pouring into a conventional filtration setup. A vacuum pump filtered out the solution to create a homogeneous hGO film. After removing the PVDF membrane, the freestanding hGO film was dried thoroughly overnight. The 3D printed GO-based meshes (geometric density ranged between 63.8 mg cm^{-3} and 108 mg cm^{-3}) were fabricated using the aforementioned printing procedure (see *Ink Preparation & 3D Printing Procedure*). Afterwards, a thermal reduction procedure was employed to fabricate Li-O_2 battery electrodes using all the aforementioned GO-based structures (3D printed meshes & VF films). The 3D printed & VF structures were placed in a closed-end quartz tube furnace. The tube furnace was then purged at room temperature (RT) with a 100 mL min^{-1} argon (Ar) flow for 20 mins before thermal reduction at 1000°C (2°C min^{-1} ramp to 1000°C followed by a 2 h isothermal hold). The reduced (3D printed mesh & VF) structures were stored in a 105°C vacuum oven overnight before cell assembly.

Li-O_2 Battery Assembly/Testing: All CR2032 cells were assembled in an Ar-filled glovebox with the thermally reduced cathode structures against a metallic lithium (Li) foil counter/reference electrode and tested using 1.0 M lithium bis(trifluoromethane)sulfonimide (LiTFSI; Sigma-Aldrich, 99.95%) in dimethyl sulfoxide (DMSO; Sigma-Aldrich, ≥99%) electrolyte (100 μL per cell). A 5/8" diameter glass fiber membrane acted as the separator between the Li foil and GO-based cathode; a 5/8" Ni foam cutout between the cathode and air cap acted as an oxygen diffusion layer, current collector, and spacer. Note that the thermally reduced structures (3D printed meshes & 2D VF films) are not flexible, but still robust enough to be handled for battery fabrication. The assembled cells were placed in a custom, air-tight jar with molecular sieves and purged with pure oxygen for at least 10 min before electrochemical measurements. The electrochemical tests were

conducted on a LAND-CT 2001A Battery Testing System. The Li-O_2 cells were cycled under controlled discharge-charge depths of 1 mAh cm^{-2} at a current density of 0.1 mA cm^{-2} from 2-4.5V. The deep discharge performance of all GO-based cathodes were also tested at 0.1 mA cm^{-2}. Note that similar cell assembly and electrochemical testing was performed on the vacuum filtrated (VF) r-hGO films for comparison purposes.

Ru Calayst Loading Procedure: The thermally reduced 3D printed electrodes were soaked for 2 h in a 8 mg mL^{-1} Ru^{3+} solution using ruthenium (III) chloride hydrate (99.9% PGM basis, Ru 38% min, Alfa Aesar) and absolute, anhydrous ethanol. After soaking, an aqueous 0.4 mg mL^{-1} sodium borohydride ($NaBH_4$) solution was prepared and slowly dropped onto the 3D printed electrodes to induce chemical reduction until no further bubbles were generated. The samples were then dried at 105°C in a vacuum oven overnight.

Post-Characterization of Disassembled Li-O_2 Cells: Li-O_2 cells in the discharge and charge states (at a curtailed depth of 1 mAh cm^{-2}) were carefully disassembled in an Ar-filled glovebox and tested using microscopic and spectroscopic techniques to determine the type of discharge products. Note that all post-characterization techniques were conducted with the Li-O_2 cathodes attached to Ni metal foam. SEM (Hitachi SU-70 field emission microscope) and Raman (Horiba Jobin Yvon LabRam ARAMIS Raman spectrometer) samples were carefully sealed and transferred to the respective chambers for characterization. A Bruker C2 Discover system with a Cu Kα radiation source was employed for X-ray diffraction (XRD) analyses. Before transferring to the XRD system, the disassembled cathode was placed on the sample stage in an Ar-filled glovebox and encapsulated with Kapton tape for protection.

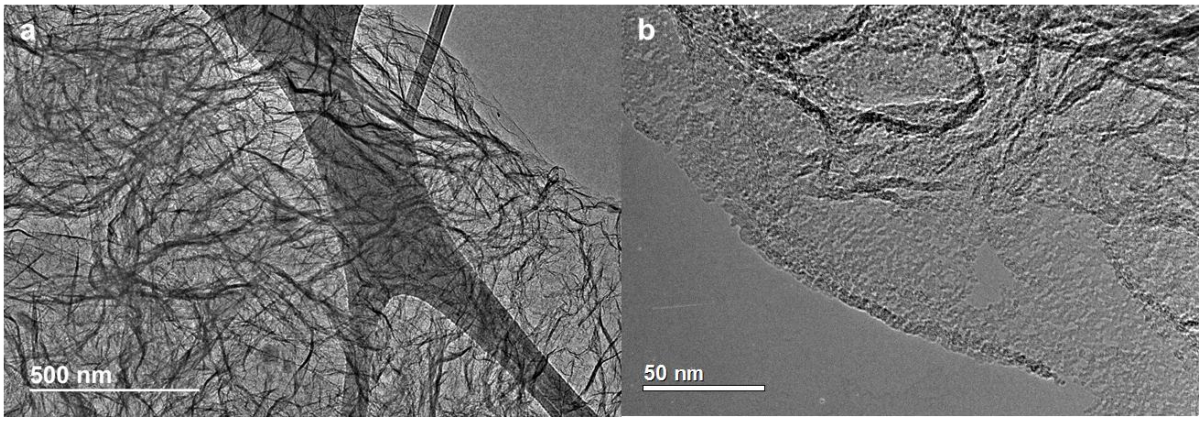

Figure S1. TEM images depicting the lateral dimensions of the hG sheets as well as the through-hole size and distribution.

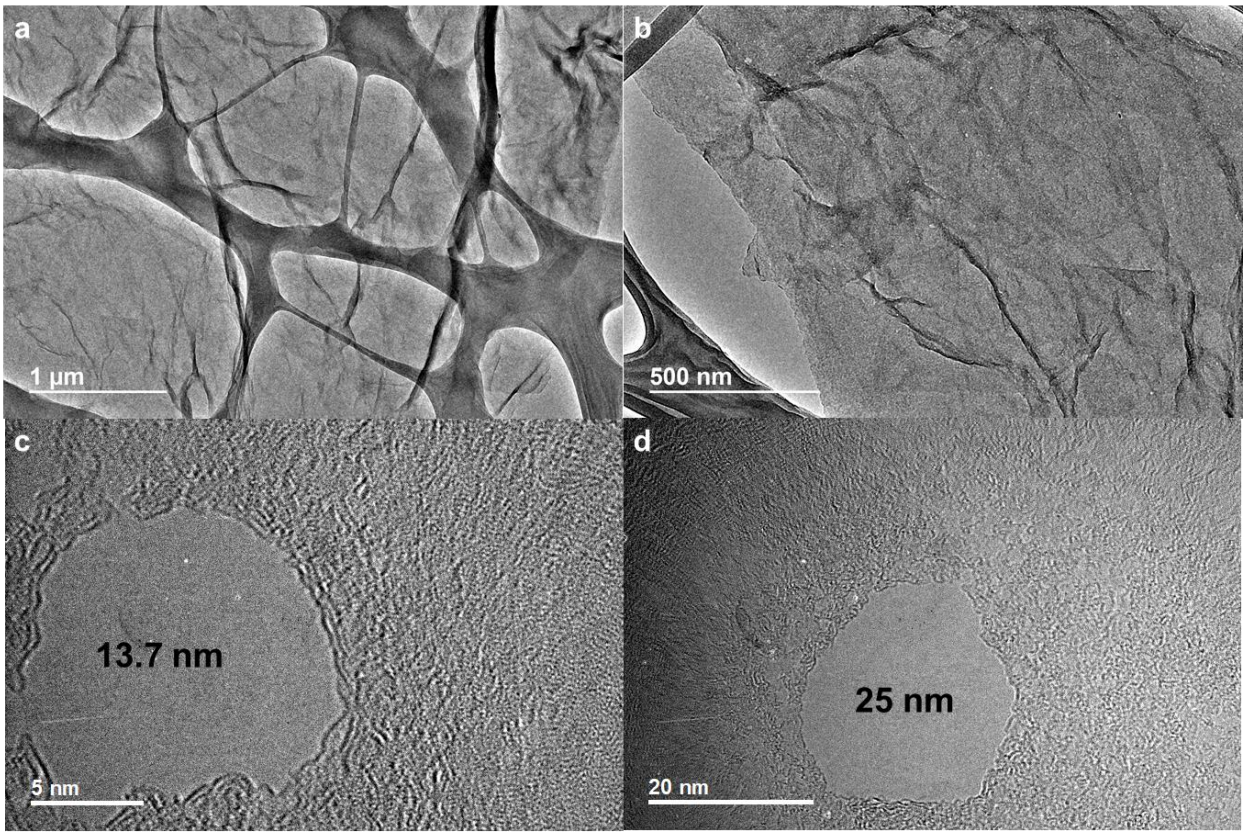

Figure S2. TEM images of the highly porous hGO material with (a-b) large lateral sheet dimensions and increased hole sizes compared to the starting hG material. The holes shown in (c)

and (d) are approximately 13.7 nm and 25 nm, respectively, which illustrates the hole diameter distribution of the hGO flakes.

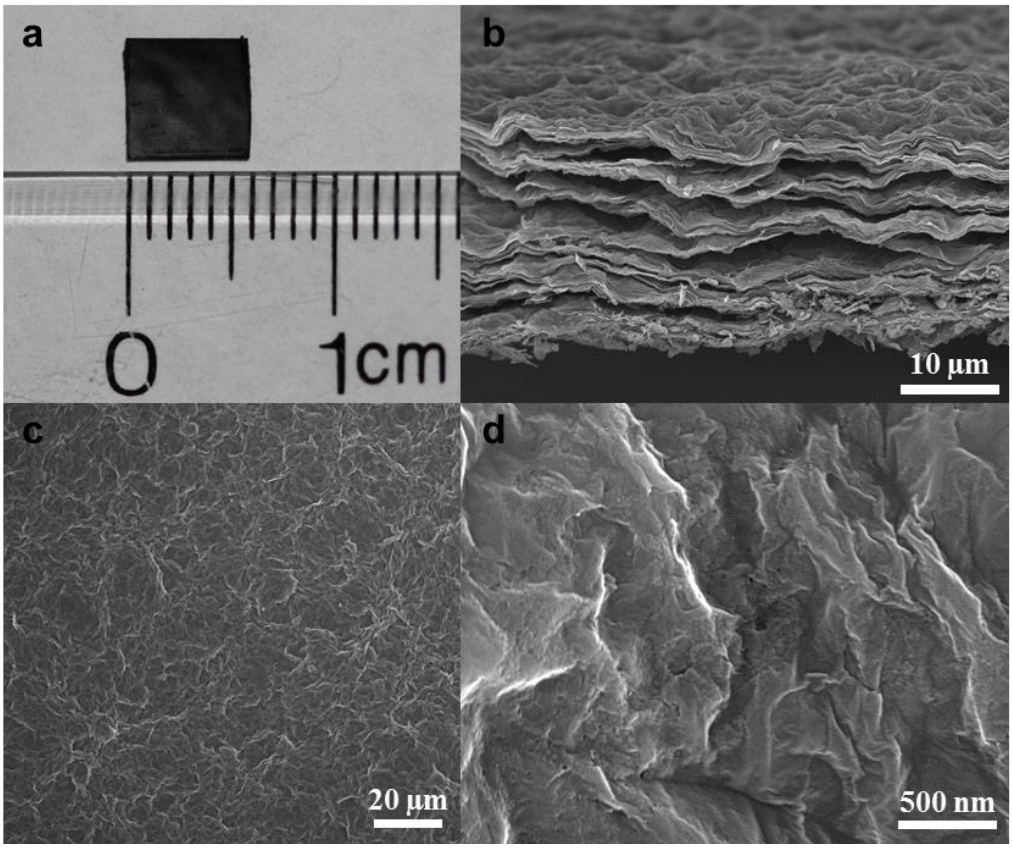

Figure S3. (a) Digital image of a vacuum filtrated (VF) hGO film after being cut to size with a razor blade. (b) Cross-sectional SEM image of the VF r-hGO film with a thickness of ~20 µm. SEM images displaying the (c) morphology and (d) hole sizes of the nanoporous VF r-hGO films used as Li-O_2 cathodes. Note that the filtration process results in a dense film with a relatively small amount of water trapped within the structure and thus, the (freeze) drying process does not provide a similar level/density of microsized pores compared to the 3D printed mesh (Figure 3 in the main manuscript).

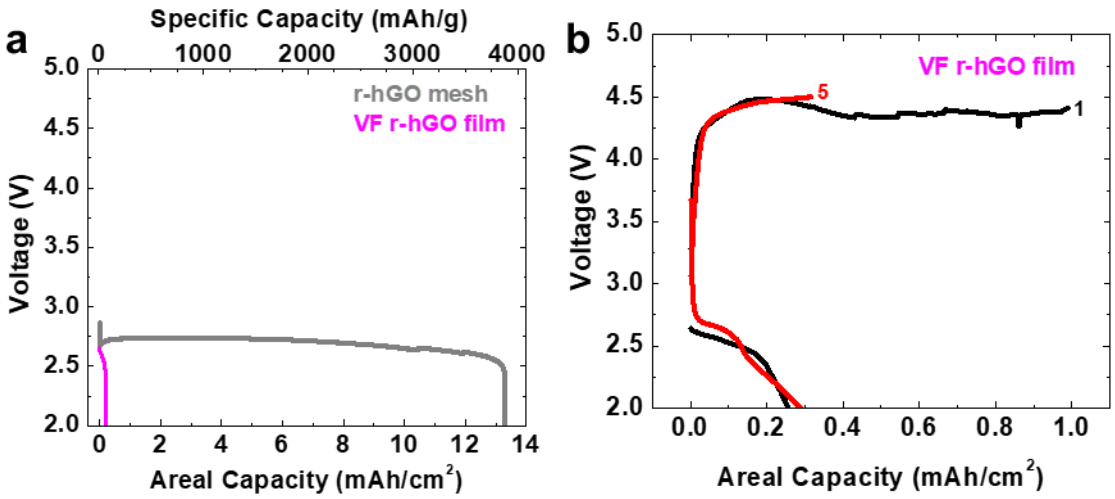

Figure S4. (a) Full discharge performance of a VF r-hGO film at 0.1 mA cm^{-2}. Compared to the 3D printed mesh, the difference is a factor of >63 and >42 in terms of areal capacity (mAh cm^{-2}) and specific capacity (mAh g^{-1}_{sample}). This clearly suggests that the micro/macroporosity provided by 3D printing (and the subsequent drying process) is the most critical in terms of capacity improvement of the air cathodes. (b) Cycling performance of a VF r-hGO film, which shows extremely limited capacity retention at the same current density. Note that additional control experiments were performed with different drying processes (freeze drying or oven drying before thermal reduction) however, there were negligible effects on the overall electrochemical performance (full discharge capacity and cyclability) of the VF film cathodes. This is due to the film's 2D structure and the nature of vacuum filtration (i.e. lack of water remaining within the VF film), which limits the accessible surface area (78 m^2 g^{-1} from the BJH method) necessary for ORR/OER reactions to occur and further proves that 3D structures are advantageous in terms of improving (Li-O_2) battery performance.

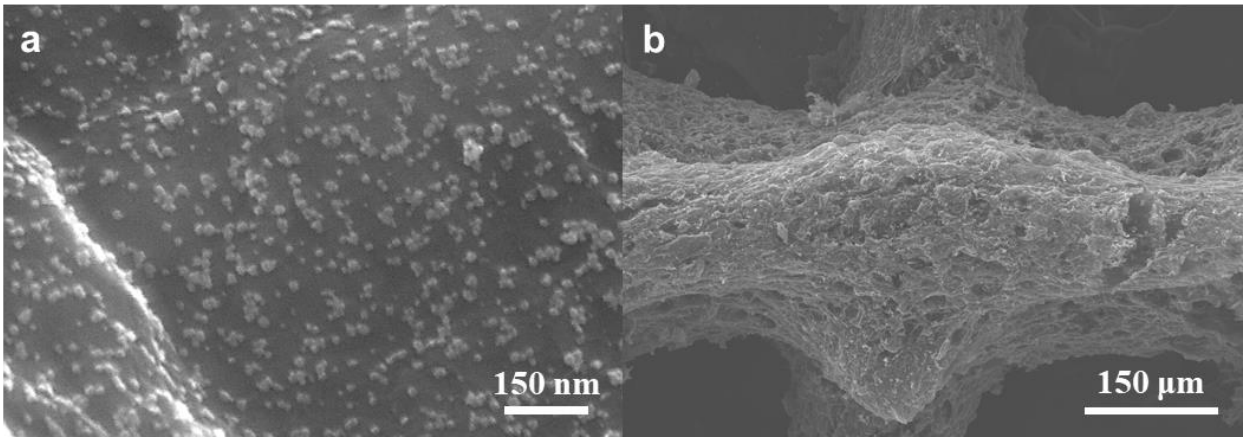

Figure S5. SEM images of the Ru/r-hGO mesh with ~10 nm particles decorating the flake surface and entire mesh structure. Note that the Ru/r-hGO mesh even after the Ru catalyst loading procedure retains the mesh structure's microscale porosity as shown in (b).

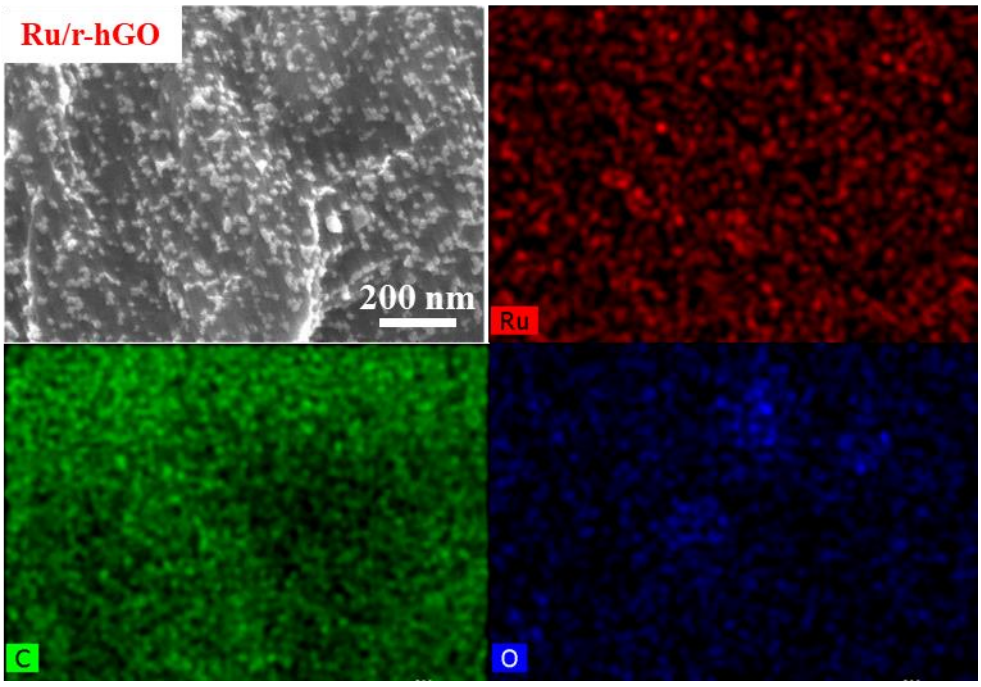

Figure S6. SEM/EDS of the 3D printed r-hGO mesh after uniformly loading metallic Ru nanoparticles.

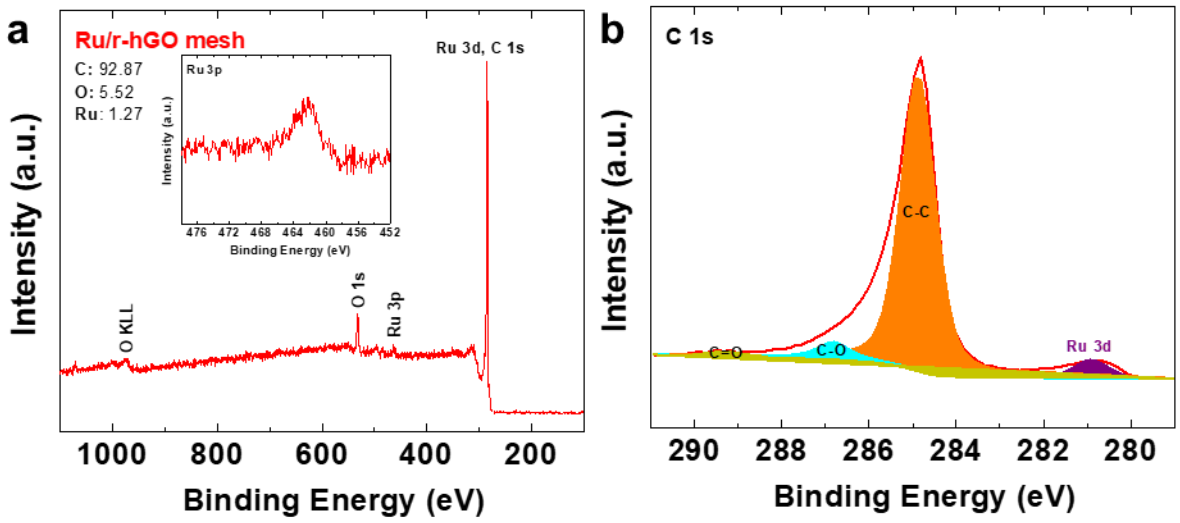

Figure S7. XPS compositional analysis of the 3D printed Ru/r-hGO mesh. (a) The full XPS spectra and (b) a higher resolution XPS scan of the C 1s peak, which shows four peaks instead of the typical three peaks for GO. The fourth peak is centered around 281 eV (purple), which corresponds to the Ru $3d_{5/2}$. The inset in (a) is a higher resolution spectra of the characteristic Ru 3p peak around 462 eV, which verifies the presence of metallic Ru NPs within the Ru/r-hGO mesh. The atomic percentages for C, O, and Ru are shown in (a), which were used to confirm the relatively low Ru loading (9.6 wt%) for the 3D printed mesh.

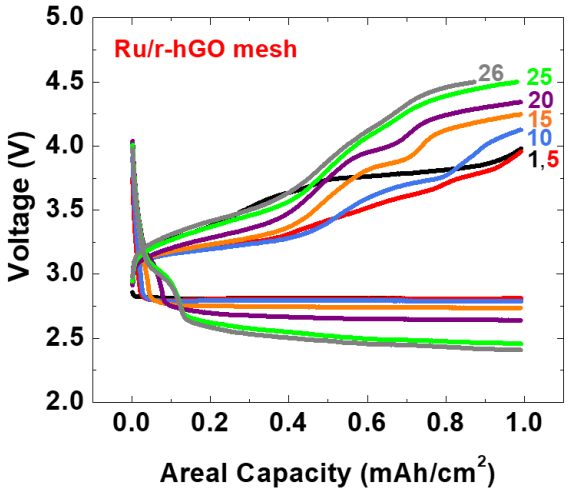

Figure S8. Controlled discharge-charge cycling depth (1 mAh cm^{-2} at 0.1 mA cm^{-2}) for a Ru-decorated 3D printed r-hGO mesh. With unoptimized catalyst loading, the Ru/r-hGO mesh displayed twice the cyclability of the r-hGO mesh.

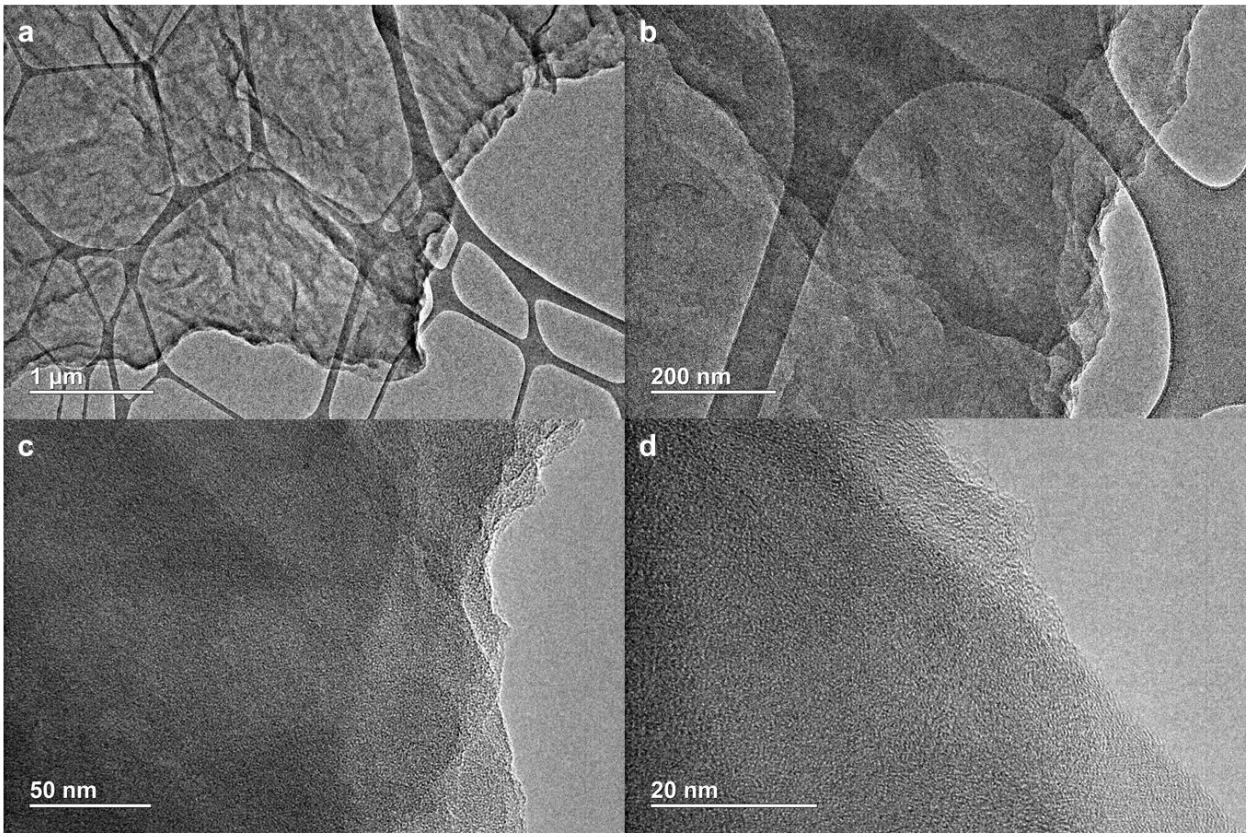

Figure S9. TEM images of a non-porous GO material synthesized using the same procedure to create hGO but with a different starting material (i.e. Vor-X graphene instead of hG). The GO from Vor-X flakes have lateral sheet dimensions of several microns or more however, even at high magnifications, no nanosized holes are observed.

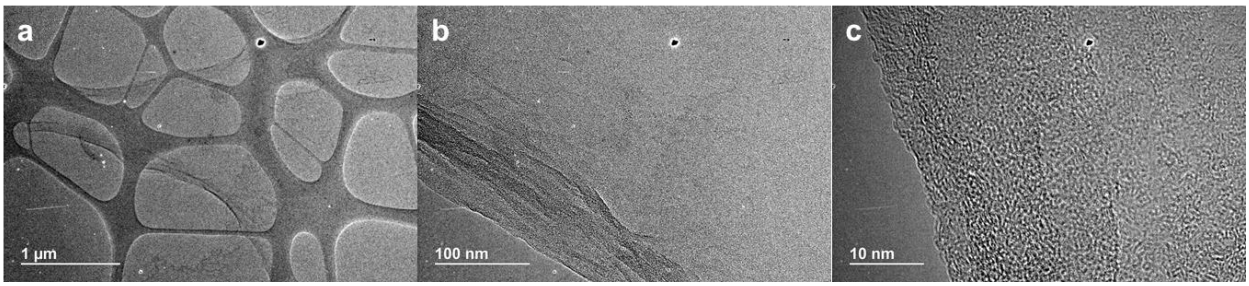

Figure S10. TEM images of GO synthesized with natural graphite as the starting material and the conventional modified Hummer's method. Similarly to the GO from Vor-X graphene, the GO from natural graphite flakes do not contain nanosized holes. Note that the dark mark is an artifact present on the CCD camera of the TEM.

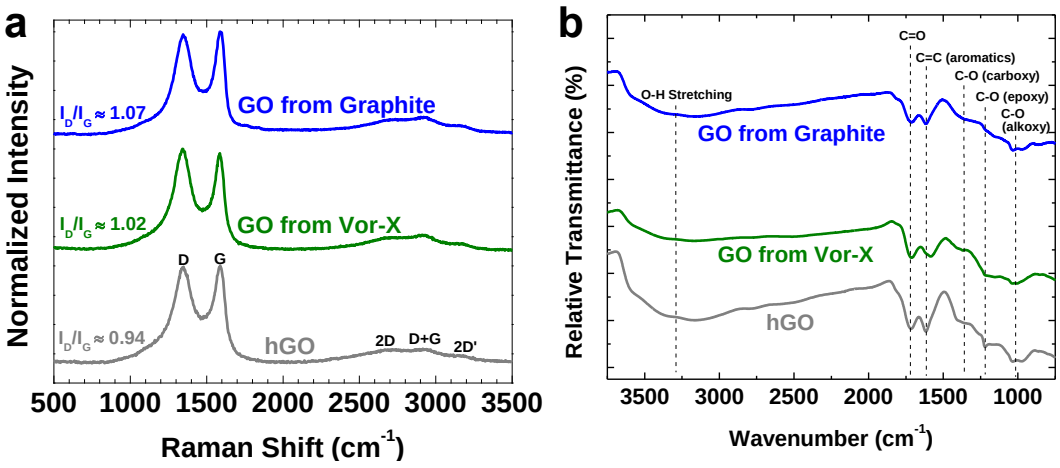

Figure S11. (a) Raman and (b) FTIR spectra of all GO-based materials: hGO, GO from Vor-X graphene and GO from natural graphite. The amount of disorder (i.e. I_D/I_G ratio) and oxygen-containing functional groups are similar between each GO-based material indicative of hydrophilicity.

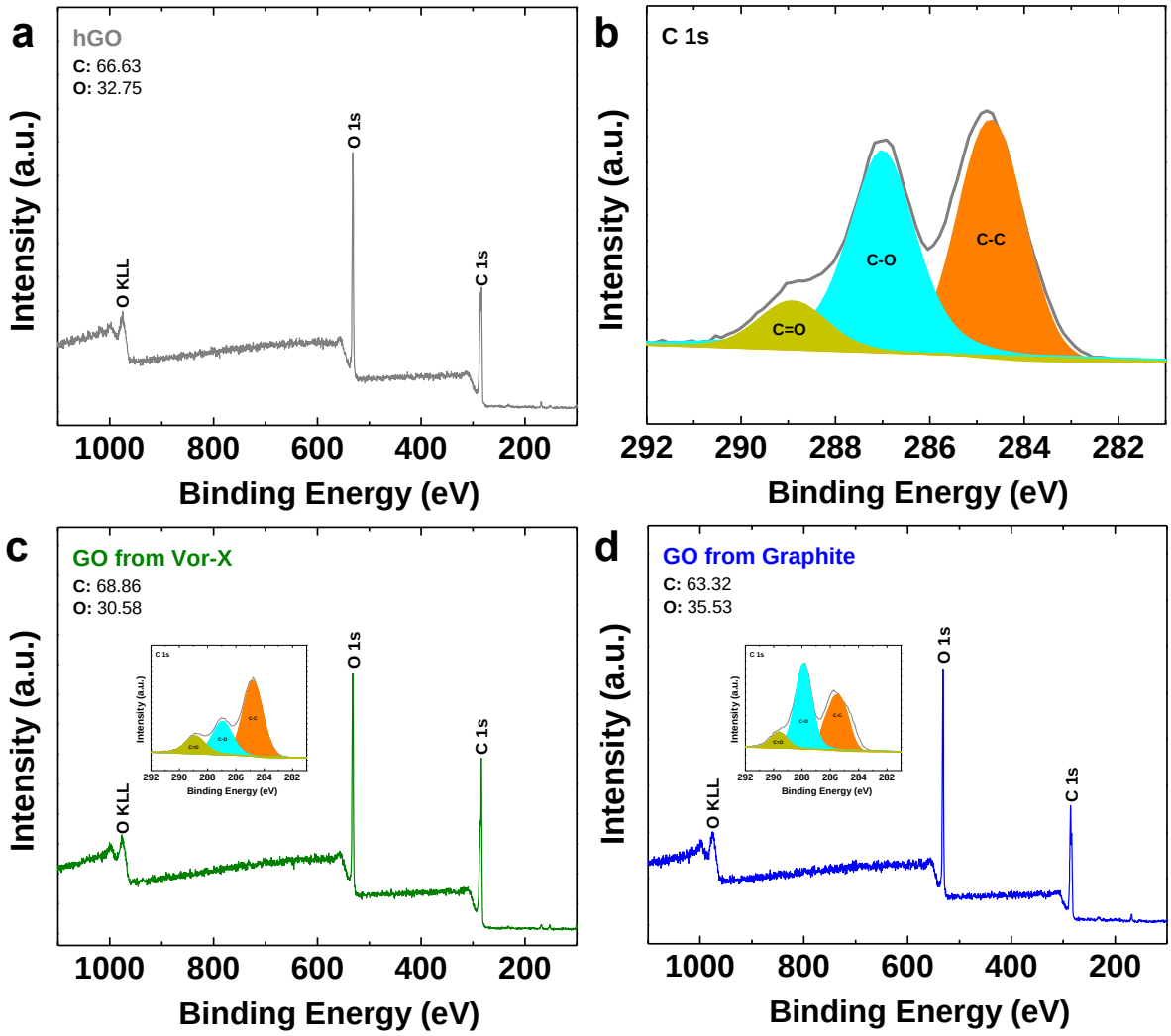

Figure S12. Compositional analysis of GO-based powders. XPS spectra of: (a) hGO, (c) GO from Vor-X graphene and (d) GO from natural graphite. Note that (b) and the insets in (c-d) are higher resolution spectra of the C 1s peak of hGO, GO from Vor-X graphene and GO from natural graphite powders, respectively, with corresponding fits to three characteristic peaks: sp^2 and sp^3 C-C at ~284.8 eV (orange), C-O around 287 eV (cyan) and C=O around 289 eV (yellow-green). Based on the atomic percentages of C and O displayed in these plots, the weight percentages for each powder were calculated: hGO powder (59.54% C and 38.98% O), GO from Vor-X graphene (60.95% C and 36.05% O), and GO from natural graphite (55.23% C and 41.29% O).

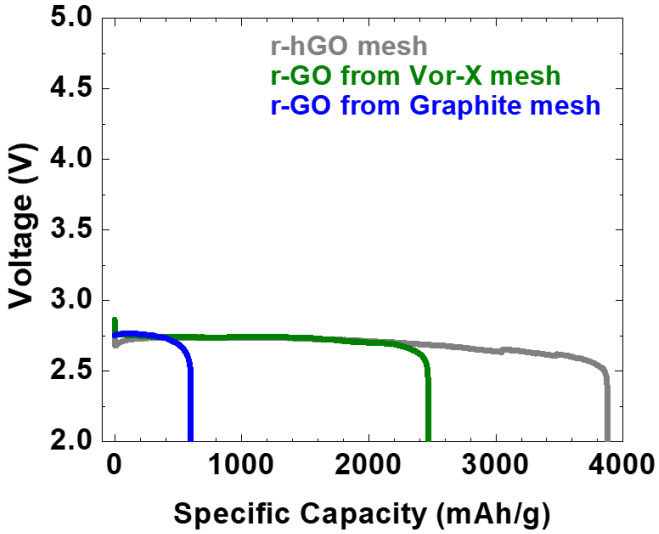

Figure S13. Deep discharge (specific capacity) performance of each 3D printed GO-based mesh Li-O_2 cathode at 0.1 mA cm^{-2}. The r-hGO mesh outperforms the other 3D printed meshes comprised of non-nanoporous GO-based materials (GO from Vor-X graphene, GO from natural graphite). Note that the specific capacity reported is mAh g^{-1}_{sample} not mAh g^{-1}_{carbon}. The 3D printed GO-based meshes have surface area values approximately 3-6 times higher than the 2D VF films.

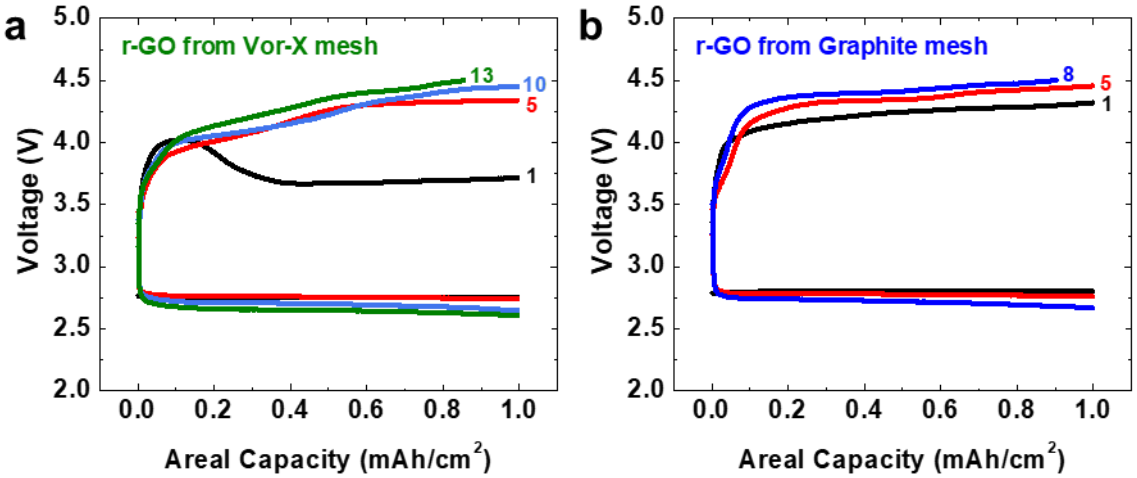

Figure S14. Controlled discharge-charge cycling depths (1 mAh cm^{-2} at 0.1 mA cm^{-2}) of 3D printed GO-based mesh cathodes without nanoporosity: (a) r-GO from Vor-X graphene, (b) r-GO from natural graphite.